Revision 1

Grain-boundary diffusion rates inferred from grain-size variations of quartz in metacherts from a contact aureole

TAKAMOTO OKUDAIRA[1,*], HIKARU BANDO[1], AND KENTA YOSHIDA[2]

[1]Department of Geosciences, Osaka City University, Osaka 558-8585, Japan

[2]Department of Mineralogy and Petrology, Graduate School of Science, Kyoto University, Kyoto 606-8502, Japan

*E-mail: oku@sci.osaka-cu.ac.jp

Running title: Grain-boundary diffusion in quartz aggregates

ABSTRACT

We evaluate a temperature-dependent coefficient for grain-boundary diffusion in quartz aggregates using grain size data from a contact aureole, based on the coupling of a numerical model for the temperature–time history of the contact aureole with a model for the kinetics of diffusion-controlled grain growth. The metachert samples were collected from the contact aureole of the Hanase–Bessho quartz diorite at Hanase Pass, Kyoto, Japan. The quartz grain sizes vary systematically with distance from the quartz diorite. We calculated the temperature–time history using a one-dimensional thermal model, validated by peak metamorphic temperature estimates that are based on the degree of graphitization of carbonaceous material in metapelites, as characterized by Raman microspectroscopy. To minimize the sum of the squares of the errors between the measured and calculated grain sizes, based on the normal grain growth law together with the temperature–time history, we estimated the activation energy and pre-exponential factor in the α-quartz field to be 208 kJ/mol and 1.1×10^{-8} m^2/s, respectively, assuming a grain boundary width of 1 nm. The grain-boundary diffusion rates for temperatures in the greenschist and amphibolite facies are similar to those determined in natural or laboratory grain coarsening experiments, but differ significantly from those determined in diffusion experiments. During grain-size-sensitive deformation, ‘effective’ grain-boundary

diffusion rates may be intermediate between the rates of diffusion along and across the grain boundary, and would be higher than the grain-boundary diffusion rates estimated by grain coarsening experiments, and lower than those by tracer diffusion experiments.

Keywords: Grain-boundary diffusion, quartz aggregates, grain sizes, contact aureole, normal grain growth

INTRODUCTION

Understanding and predicting the rheological behavior of many common crustal rocks requires knowledge of the mechanical properties of quartz crystals and aggregates, because quartz is one of the most abundant rock-forming minerals in the Earth's continental crust. Diffusion contributes to most of the important deformation mechanisms, including grain-size-sensitive diffusion creep/grain-boundary sliding and insensitive dislocation creep (e.g., Okudaira and Shigematsu 2012). In order to evaluate the relative importance of these different mechanisms for quartz deformation, the diffusion kinetics of the major ionic species in quartz crystals and aggregates must first be known.

The grain-boundary (or bulk) diffusion coefficients of Si or O have been estimated from tracer diffusion experiments (Farver and Yund 1991a, 2000a), and from natural or laboratory grain-coarsening experiments (Joesten 1983, 1991; Tullis and Yund 1982).

According to Farver and Yund (2000a), based on the data obtained by isotopic tracer (^{30}Si) and standard step-scan analysis using an ion microprobe, the temperature dependence of silicon bulk diffusion in novaculite for hydrothermal experiments at 600–800 °C and 150 MPa confining pressure, and dry experiments at 800–1100 °C and 1 atm (in a stream of dry N_2), respectively, is described by the Arrhenius parameters D_0 = 3.7×10^{-10} m^2/s and E = 137 ± 18 kJ/mol, and D_0 = 6.2×10^{-9} m^2/s and E = 178 ± 38 kJ/mol. Assuming volume diffusion to be negligible (i.e., type C kinetics; Saal et al. 1990), the measured bulk diffusion rates (D_{bulk}) can be related to grain-boundary diffusion rates (D_{gb}) through the expression $D_{bulk} = \tau D_{gb}\delta/d$, where τ, the tortuosity factor, represents the ratio of the true path length to the length of the measured profile (e.g. Watson 1991), δ is the grain-boundary width, and d the average grain size. The value of τ depends on the grain geometries, and estimates typically range from 1.5 to 2.0 (e.g., Farver and Yund 2000a).

On the other hand, variations in the grain-sizes of quartz in five nodular chert samples from the Christmas Mountains contact aureole were matched by a normal grain growth model in which the temperature dependence of the Arrhenius function, along a temperature–time history, was calculated by one-dimensional thermal modeling (Joesten 1983). Assuming a grain boundary width of 1 nm, the data permit the coefficient for the

grain-boundary diffusion of oxygen in quartz aggregates to be estimated as $D = 8.07 \times 10^{-10} \exp(-210 \times 10^3/RT)$ for the temperature range of 600–1000 °C. Tullis and Yund (1982) determined grain growth rates for quartz aggregates between 800 °C and 1000 °C at 200–1500 MPa, and based on the data from a grain-growth experiment of Tullis and Yund (1982), Joesten (1991) recalculated the values of D_0 and E as 5.23×10^{-7} m^2/s and 282 kJ/mol, respectively.

The values of the grain-boundary diffusion coefficients extrapolated to the conditions of greenschist to granulite facies (~300–900 °C) are ~10^{-19} to 10^{-12} m^2/s (wet experiment of Farver and Yund 2000a), ~10^{-21} to 10^{-13} m^2/s (dry experiment of Farver and Yund 2000a), ~10^{-29} to 10^{-19} m^2/s (Joesten 1983), and ~10^{-30} to 10^{-18} m^2/s (Joesten 1991, based on the data of Tullis and Yund 1982); there is a significant difference between the coefficients for a quartz aggregate calculated from diffusion and grain-coarsening experiments.

The phenomenological, isothermal kinetic grain-growth equation is given by

$$d^n - d_0^n = K_0 \exp(-E / RT)t \quad (1)$$

where d is the average grain size (m) at time t (s), d_0 is the initial grain size, n is the kinetic

grain-growth exponent, K_0 is a pre-exponential constant (m^n/s), E is the activation energy for grain growth (J/mol), R is the gas constant (J/mol/K), and T is temperature (K). Where pores and impurities are absent, theoretical considerations predict a value of $n = 2$ in a pure single-phase system, and the grain growth is controlled by the diffusion of atoms across the grain boundary (e.g., Joesten 1991 and references therein). Thus, grain growth is a diffusional process, and the analysis of natural or laboratory coarsening experiments can yield values for the grain-boundary diffusion coefficients.

The intrusion of a quartz diorite (2.6×1.6 km in surface area) in the Hanase–Bessho area, Kyoto, Japan, produced an extensive contact aureole (Fig. 1; Kiji et al. 2000; Kimura et al. 1998, 2001). Thermally metamorphosed rocks derived from chert, mudstone, and sandstone crop out along a roadside, and extend 1600 m normal to the contact with the quartz diorite. The average grain-size of quartz in the cherts increases systematically towards the quartz diorite contact. In our study of these cherts, similar to the analysis of Joesten (1983), we evaluate the temperature-dependent coefficient for grain-boundary diffusion in the quartz aggregates, using grain-size data from the contact aureole. We also couple a numerical model of the temperature–time history of the contact aureole with a model of the kinetics of diffusion-controlled grain growth.

METHODS AND SAMPLES

Method

Isothermal grain growth in a single-phase aggregate can be described by an equation of the following form (Joesten 1983, 1991; Rubie 1986):

$$d^2 - d_0^2 = \frac{8\gamma V_m}{RT}\frac{D_0}{\delta}\exp(-E/RT)t \quad (2)$$

where γ is the surface energy (J/m^2), V_m is the molar volume (m^3/mol), D_0 is the pre-exponential factor (m^2/s), and δ is the grain-boundary width (m). When temperature is a function of time, such as in a contact aureole, rocks at any point in the aureole experience a heating–cooling cycle, the magnitude and duration of this cycle are functions of the distance from the intrusive contact, and all terms in T are included within the time integral, so that

$$d^2 - d_0^2 = \frac{8\gamma V_m}{R}\frac{D_0}{\delta}\int_{t_0}^{t}\frac{1}{T(t)}\exp\left(-E/RT(t)\right)dt \quad (3)$$

The grain size at a given distance from the intrusive contact is a function of both temperature and time. For thermally activated grain growth, all the information relating to

121 the temperature dependent behavior of the system is included within the
122 temperature–time integral. The temperature–time integral at a given distance from the
123 contact can be evaluated numerically using a thermal model for the contact aureole.
124 Assuming a constant duration of grain growth of quartz at any distance from the intrusive
125 contact, the average temperature at a given distance from the contact can be calculated by
126 dividing the T–t integral by the duration of grain growth; i.e., the average temperature
127 over time. If the grain-growth exponent of 2 is independent of temperature, it can be used
128 to obtain first-order approximations of the activation energy and the pre-exponential
129 factor for quartz grain growth, which can be determined from the slope of an Arrhenius
130 plot of $\ln[(d^2 - d_0^2)T]$ versus $1/T$. In this case, T means the average temperature at a given
131 distance from the intrusive contact, as defined by dividing time-integrated temperatures
132 by a particular period at any point in the aureole. Furthermore, we calculate the values of
133 the activation energy and pre-exponential factor more precisely, to minimize the sum of
134 the squares of the errors between the measured and calculated grain sizes, using Equation
135 3 along with the temperature–time history.

136 We evaluate the temperature–time history of the contact aureole with a
137 one-dimensional thermal model, assuming a sheet-like shape for the intrusion. A
138 one-dimensional heat transfer equation can be written as

$$\frac{\partial T}{\partial t} = \frac{K}{\rho_m C_m}\frac{\partial^2 T}{\partial x^2} + \frac{A}{\rho_m C_m} \quad (4)$$

where ρ_m is the density of the rock (kg/m^3), C_m is the specific heat of the rock (J/kg/K), K is the thermal conductivity (W/m/K), x is a horizontal coordinate (m) measured from the center of the quartz diorite body, and A is the heat produced by radioactive elements (W/m^3). Equation 4 was solved numerically using an explicit finite-difference method with an array spacing (Δx) of 10 m and a time step (Δt) of 3.15×10^7 s. The production of heat during crystallization of the magma (i.e., latent heat) has been calculated to be continuous linear functions of temperature during the interval of crystallization between the liquidus and solidus temperatures. The production of heat was incorporated into the numerical model using an effective heat capacity (C^*) and an effective thermal diffusivity (κ^*) for rocks undergoing these reactions (e.g., Hanson and Barton 1989). The effective thermal diffusivity is then calculated from

$$\kappa^* = \frac{K}{\rho_m C^*} \quad (5)$$

where C^* is defined by

157

158 $$C^* = C_m + \left[\Delta H_{magma} / (T_{liq} - T_{sol}) \right] \quad (6)$$

159

160 where ΔH_{magma} is the enthalpy of the crystallizing magma (J/kg), T_{liq} is the liquidus
161 temperature, and T_{sol} is the solidus temperature. The values of parameters used in the
162 numerical simulation are listed in Table 1. In this study, we assumed no magmatic
163 convection or recharge.

164

165 **Samples**

166 We collected metachert samples from the contact aureole around the Late Cretaceous
167 Hanase–Bessho quartz diorite (Kiji et al. 2000). The quartz diorite is massive and
168 medium-grained, and it is composed mainly of plagioclase, quartz, hornblende, biotite,
169 and K-feldspar, with minor amounts of titanite, opaque minerals, and apatite. The SiO_2
170 content of the bulk-rock is ~66–67 wt.% (Kiji et al. 2000). The quartz diorite has steeply
171 dipping contacts with country rocks (Kimura et al. 2001), and is likely to be a sheet-like
172 or tabular intrusion. The contact aureole has a width of up to around 1 km, and it is
173 recognized on the basis of the occurrence of metamorphic biotite in the metasediments.
174 Away from the contact aureole, the rocks are characterized by the mineral assemblage

muscovite + chlorite. Samples next to the intrusive contact (<~180 m) contain cordierite that is partially or totally pinitized, and the characteristic assemblage is cordierite + biotite. Along the road where our samples were taken, biotite is present up to 710 m from the intrusive contact. We could not collect metachert samples close to the intrusive contact along the main road, and for this reason, the four samples closest to the intrusive contact had to be collected from a different area.

Grain size analysis

The grain sizes of the recrystallized quartz were measured using the image analysis software ImageJ. Each grain size was calculated as the equivalent circular diameter of a grain, and the mean grain size was calculated as the arithmetic mean of the log of grain sizes, or in other words, the geometric mean grain size. We analyzed optical photomicrographs to measure the grain sizes of quartz in sample A. The grain boundaries of minerals were manually traced on photomicrographs taken under plane and crossed-polarized light. To measure the grain sizes of fine-grained quartz in some samples, we analyzed secondary-electron images obtained with a scanning electron microscope (SEM) at the Department of Geosciences, Osaka City University, Japan. We used 200–900 grains in each sample to measure the mean grain size of the quartz. The

193 modal amounts of minerals were also determined during the analysis, and the analytical
194 results are listed in Table 2.
195
196 **RESULTS**
197 **Results of thermal modeling**
198 Results of the thermal modeling are shown in Figure 2; the temperature profiles are
199 shown for each elapsed time, as well as the maximum temperature experienced by a rock
200 at any position in the aureole. The results of the thermal modeling have been verified by
201 temperature estimates based on the degree of graphitization of carbonaceous material in
202 the metapelites using Raman microspectroscopy (e.g., Aoya et al. 2010; Beyssac et al.
203 2002). The degree of graphitization of the carbonaceous material is not affected by
204 retrogression, and it records the peak metamorphic conditions. The spectroscopy was
205 carried out with the laser Raman spectrometer (JASCO NRS-3100) at Kyoto University,
206 Japan, using the 514.5 nm line of an Ar–ion laser at $20–30 \times 10^{-3}$ W, and a spot size of 1
207 μm on the sample surface. We analyzed the relative area of the defect band, i.e., the
208 D1/(G + D1 + D2) peak area ratio (R2 ratio), where D1, D2, and G bands occur at 1350,
209 1620, and 1580 cm^{-1}, respectively, and calculated the peak temperature with the equation
210 T (°C) = $–445 \times R2 + 641$ (Beyssac et al. 2002). Although the degree of graphitization of

carbonaceous material would be affected by not only the temperature but also the duration of the temperature, the relationship between temperature and the degree of graphitization of carbonaceous material for regional metamorphic rocks (Beyssac et al. 2002) is applicable to contact metamorphic aureoles (Aoya et al. 2010). The calculated temperatures for the metapelites (see Table 3) are 570 ± 32 °C (182 m from the contact), 536 ± 34 °C (573 m), 471 ± 25 °C (1136 m), and 470 ± 32 °C (1400 m). The results (see Fig. 2b) are comparable to the maximum temperatures obtained by thermal modeling, indicating that the temperature profiles calculated by the model are suitable for studying the thermal structure and temperature–time (*T*–*t*) history of the rocks around the Hanase–Bessho quartz diorite. In this thermal model, the duration of the high-temperature conditions is a minimum estimate, because we do not consider magmatic convection or recharge. Consequently, the diffusion rates estimated for the inferred *T*–*t* history are maximum estimates.

Results of grain size analysis

The quartz grains studied are polygonal and equigranular (Fig. 3a), and there are no microstructures indicative of internal plasticity. The grain size distributions of the quartz in the metacherts are log-normal (Fig. 3b), and the results of quartz grain-size

229 measurements are shown in Figure 4 and Table 2. The quartz grain size increases towards
230 the intrusive contact, but the observed data do not fit the expected exponential variation
231 with distance from the contact, and the grain growth of quartz near the contact seems to
232 have been inhibited. The modal amounts of second-phase minerals (mainly sheet silicates
233 and carbonaceous materials) in the metacherts near the contact are approximately 3–4
234 vol.% (Table 2), slightly more than in the other samples, except for sample 110331-22.
235 This result suggests that the presence of second-phase minerals has an effect on the grain
236 growth kinetics of the first-phase quartz, resulting in the pinning or dragging of quartz
237 grain boundaries, with the pinning process ensuring that the grain size remains small. The
238 grain size of the first-phase mineral is strongly dependent on the grain size (d_p in microns)
239 and volume fraction (f_p) of the second-phase minerals: the ratio d_p/f_p is referred to as the
240 Zener parameter or Zener ratio, Z (e.g., Brodhag et al. 2011; Herwegh et al. 2011). At low
241 Z values, grain growth of the first-phase mineral is controlled by the pinning effect of the
242 second-phase minerals (i.e., second-phase controlled coarsening regime) and the upper
243 limit of Z values of this regime increases with increasing temperature. The effect of the
244 second-phase minerals on normal grain growth of the first-phase mineral is smaller at
245 lower temperatures than at higher temperatures. In samples collected farther from the
246 intrusion contact, the second-phase minerals are several microns in size, and their Z

values are calculated to be ~10^2–10^3 μm, suggesting a negligible effect of the second phases on grain growth of the first phase (e.g., Herwegh et al. 2011; Okudaira et al. 2010). In samples from near the intrusion contact, the grain sizes of the second-phase minerals are large (up to ~10–20 μm) and the calculated Z values are ~10^2–10^3 μm, which are similar to the Z values of samples collected farther from the contact. Because the Z values of samples from near the intrusion contact (i.e., high-temperature samples) may fall within the field of the second-phase controlled coarsening regime, the effect of the second phases on grain growth of the first-phase quartz would be higher than in other samples, although to an unknown degree.

DISCUSSION

Estimates of activation energy and the pre-exponential factor

To obtain first-order approximations of the values of the activation energy and the pre-exponential factor, we have constructed an Arrhenius plot of $\ln[(d^2 - d_0^2)T]$ for metachert data and reciprocal temperatures, as shown in Figure 5. The growth period in this case is 25×10^3 years, a figure that was chosen arbitrarily as the period during which the temperatures at the center of the intrusion fell to 500 °C (see Fig. 2), after which time the temperature profiles are nearly constant. The solid line in this figure is a linear least

squares fit for the 17 data given by $\ln[(d^2 - d_0^2)T] = 11.123 - 19698/T$ ($r^2 = 0.87772$). The activation energy for quartz grain growth is 163.8 ± 15.8 kJ/mol. Assuming a grain boundary width of 1 nm, the pre-exponential factor is estimated to be 1.2×10^{-11} m^2/s. Excluding three samples (open circles in Fig. 5) near the intrusion contact when estimating the activation energy and the pre-exponential factor, a linear least squares fit for the remaining 14 data points yields $\ln[(d^2 - d_0^2)T] = 17.919 - 24638/T$ ($r^2 = 0.91442$). The activation energy and the pre-exponential factor are 204.8 ± 18.1 kJ/mol and 1.1×10^{-8} m^2/s, respectively.

To estimate the values of the activation energy and the pre-exponential factor more precisely, we calculated quartz grain sizes using Equation 3, together with the temperature–time history, in order to make comparisons with measured grain sizes (Fig. 6). To minimize the sum of the squares of the errors between the calculated and measured grain sizes, the values of the activation energy and pre-exponential factor, respectively, should be 132 kJ/mol and 4.8×10^{-14} m^2/s. We obtained a grain-boundary diffusion rate of $D_{gb} = 4.8 \times 10^{-14} \exp(-132/RT)$. The value of the activation energy agrees with the value of 137 ± 18 kJ/mol, determined by Farver and Yund (2000) for the bulk diffusion of silicon or grain-boundary diffusion in wet quartz aggregates. The pre-exponential factor differs significantly from the figure of 2.2×10^{-6} m^2/s that is given by Farver and Yund

283 (2000a) for experimental grain-boundary diffusion in wet quartz aggregates, assuming a
284 tortuosity factor $\tau = 1.7$ and a ratio of grain-boundary width to grain size $\delta/d = 0.0001$.
285 Excluding three samples (open circles in Fig. 6) near the intrusion contact, the activation
286 energy and pre-exponential factor are 208 kJ/mol and 1.1×10^{-8} m^2/s, respectively. The
287 value of the activation energy agrees with the value of 210 kJ/mol reported by Joesten
288 (1983).

289 The values for the activation energy and pre-exponential factor of quartz grain
290 coarsening that we have determined may be controlled by silicon grain-boundary
291 diffusion. When water is present, Farver and Yund (2000a) suggested that grain-boundary
292 diffusion accommodated processes in quartz aggregates will most likely be rate-limited
293 by the transport of silicon, because the rate of oxygen grain-boundary diffusion is greater
294 than silicon grain-boundary diffusion by a factor of about 2. The metachert samples
295 studied here contain small amounts of sheet silicates (muscovite, chlorite, and/or biotite),
296 and therefore at least trace amounts of water or water-related species were present at the
297 time of contact metamorphism.

298 The volume diffusion coefficients of O in α- and β-quartz under hydrothermal
299 conditions are significantly different (Fig. 7; Farver and Yund 1991b; Giletti and Yund
300 1984), and then the grain-boundary diffusion coefficients of Si may be different between

the stability fields of α- and β-quartz. In the present study, quartz in samples from near the intrusion contact (within ~180 m) does not show the expected exponential variation in grain size with distance from the contact. Given that the temperature conditions of the α–β transition in quartz at a confining pressure of 200–300 MPa are 630–650 °C (Shen et al. 1993), at least near the metamorphic peak, the growth of quartz grains in these samples must have occurred in the β-quartz field. The suppression of grain growth may have resulted from the fact that the grain-boundary diffusion coefficients for the β-quartz field are different from those for the α-quartz field. In the β-quartz field, the volume diffusion rates of O calculated using diffusion coefficients for β-quartz are slower than those calculated using diffusion coefficients for α-quartz, because the extrapolated volume diffusion rates of O in α- and β-quartz for the entire temperature range, as calculated from diffusion rates for experimental temperature range (see Fig. 7), cross over near the temperature of the α–β transition (Farver and Yund 1991b; Giletti and Yund 1984). Therefore, in the β-quartz field, the grain-boundary diffusion rates of Si calculated using grain-boundary diffusion coefficients for β-quartz are likely to be slower than those calculated using diffusion coefficients for α-quartz. The grain size of quartz in β-quartz aggregates is larger when calculated using the grain-boundary diffusion coefficients for the α-quartz field, than when calculated with diffusion coefficients for the β-quartz field.

This means that the difference between the grain size of quartz in samples from near the intrusion contact and the expected exponential variation with distance from the contact can be attributed to the difference in the grain-boundary diffusion coefficients of Si in the α- and β-quartz fields. However, because no previous experiment has considered grain-boundary diffusion in the α-quartz field, we cannot conclude that the grain-boundary diffusion coefficient of Si differs between the α- and β-quartz fields.

The calculated grain size variations, using the *T*–*t* history and different diffusion rates, are shown in Figure 6 in order to compare them with the measured grain size variations. The calculated grain size variations, using the values for D_0 and E for the bulk diffusion of silicon, given by Farver and Yund (2000a), are much larger than the measured grain size variations, suggesting that the Farver and Yund (2000a) values of D_0 and E cannot be applicable to the grain coarsening of quartz in natural quartz aggregates under the conditions of the greenschist and amphibolite facies.

Grain-boundary diffusion rates in quartz aggregates

Figure 7 shows the diffusion rates for quartz aggregates estimated in this study and previous studies. In this figure, the grain-boundary width is assumed to be 1 nm. Using our estimated values of the activation energy and pre-exponential factor, the

337 grain-boundary diffusion rates for temperatures in the greenschist and amphibolite facies
338 are similar to those of Joesten (1983), as well as those of Tullis and Yund (1982), whose
339 values have been recalculated by Joesten (1991), but they differ significantly from those
340 of Farver and Yund (2000a) (Fig. 7). The grain-boundary diffusion rates estimated from
341 studies of grain coarsening (Joesten 1983; Tullis and Yund 1982; this study) are about
342 four to six orders of magnitude smaller than the silicon grain-boundary diffusion rates
343 determined by Farver and Yund (2000a). The difference between the measured silicon
344 grain-boundary diffusion rates and the values obtained from grain coarsening studies may
345 be due to several factors.

346 The results from experimental studies typically yield a grain coarsening exponent
347 significantly greater than 2, indicating that abnormal grain growth has occurred, possibly
348 because of grain-boundary drag due to the presence of secondary phases, pores, or
349 contaminants, or possibly because the coarsening is by an Ostwald ripening mechanism
350 instead of normal grain growth (Farver and Yund 2000a). In either case, the apparent
351 grain-boundary diffusion rates estimated from the grain coarsening experiments would be
352 much slower than the true value. However, judging from the values of the coefficient of
353 determination (r^2) for least squares regression to fit the data, a kinetic grain-growth
354 exponent (n) of 2 is the most suitable for the present data set, rather than n = 3 or 4,

355 suggesting that normal grain growth is the most likely control of quartz grain sizes in the
356 contact aureole.

357 As described above, the volume diffusion rate of O is much lower in α-quartz than in
358 β-quartz (Fig. 7; Farver and Yund 1991b; Giletti and Yund 1984). The grain-boundary
359 diffusion rates estimated by Farver and Yund (2000a) were measured in the β-quartz field,
360 whereas those of the present study were estimated mainly in the α-quartz field.
361 Consequently, the difference between the two sets of grain-boundary diffusion rates can
362 be attributed to differences in the diffusion coefficients in the α- and β-quartz fields.
363 However, if the grain-boundary diffusion rates in the β-quartz field are much higher than
364 those in the α-quartz field, then we would expect the grain size of quartz in samples from
365 near the intrusion contact to be much larger than in samples farther from the contact, yet
366 this is not the case. Furthermore, the difference in grain-boundary diffusion rates between
367 Farver and Yund (2000a) and the present study is much larger than the difference in the
368 volume diffusion rate of O between α- and β-quartz. The grain-boundary diffusion rates
369 measured in the β-quartz field, in grain-coarsening experiments (Joesten 1991; Tullis and
370 Yund 1982), differ significantly from those of Farver and Yund (2000a). Thus, the
371 difference between the grain-boundary diffusion rates of Farver and Yund (2000a) and
372 those of the present study cannot be attributed to differences in the grain-boundary rates

373 between α- and β-quartz.

374 Dohmen and Milke (2010) summarized Si grain-boundary diffusion data for quartz
375 (Farver and Yund 2000a), Mg_2SiO_4 polymorphs (Farver and Yund 2000b; Shimojuku et al.
376 2009), and $MgSiO_2$ perovskite (Yamazaki et al. 2000). While the diffusion properties of
377 grain boundaries in Mg_2SiO_4 and $MgSiO_3$ high-pressure phases are nearly identical when
378 pressure dependence is considered, the data for quartz are strikingly different, with
379 grain-boundary diffusion rates of quartz being 4–5 orders of magnitude higher than those
380 of Mg_2SiO_4 and $MgSiO_3$ high-pressure phases. This difference may be related to the
381 different grain-boundary structures and the diffusion mechanism of Si (due to the
382 presence of Mg), or related to effectively wet grain boundaries even in nominally dry
383 studies. Dohmen and Milke (2010) reported that the water contents of the natural
384 novaculite samples analyzed by Farver and Yund (2000a) were not measured before or
385 after the experiments. Even in the dry experiment (in a N_2 stream), water might have
386 initially been present along grain boundaries in the samples, thereby influencing Si
387 diffusivity. Since hydrogen is an incompatible element in most minerals, it is likely to
388 become concentrated along grain boundaries, strongly affecting the grain boundary
389 structure. In fact, based on the experimentally determined growth rates of wollastonite
390 reaction rims between quartz and calcite (where small amounts of water are always

present), the grain boundary diffusion rates of SiO_2 are 10^{-16} to 10^{-14} m^2/s at 850 to 1000 °C, assuming a grain boundary width δ = 1 nm (Milke and Heinrich 2002). These rates are comparable to those reported for Si bulk diffusion in dry and wet experiments performed by Farver and Yund (2000a), whereas Milke and Wirth (2003) reported diffusion rates of 10^{-16} to 6×10^{-18} m^2/s (950 to 850 °C) for SiO_2 in wollastonite rims from completely dry experiments in a CO_2 atmosphere, being almost two orders of magnitude lower than the rates obtained by Milke and Heinrich (2002). However, in the metachert samples studied here, small amounts of sheet silicates are observed (e.g., muscovite, chlorite, and/or biotite), suggesting that at least trace amounts of water or water-related phases were present at the time of contact metamorphism. Thus, the difference between the grain-boundary diffusion rates of Farver and Yund (2000a) and those of the present study cannot be attributed to differences in the amount of water at grain boundaries.

In natural rocks, the grain-boundary width ranges from several to tens of nanometers (Nakashima 1995). The effective grain boundary width is a poorly constrained measure that acts in opposite directions in the derivation of diffusion coefficients from grain coarsening or diffusion experiments. Grain-boundary diffusion rates depend on the factor D_{gb}/δ in grain coarsening experiments, whereas the grain-boundary diffusion coefficient

409 is estimated by the relation $D_{bulk} = \tau D_{gb}\delta/d$ in tracer diffusion experiments. When the
410 grain boundary width is 10 nm, D_{gb} for grain coarsening experiments increases by an
411 order of magnitude, and that for tracer diffusion experiments decreases by an order of
412 magnitude; consequently, the difference in diffusion rate between them decreases by two
413 orders of magnitude. The rate-limiting jump distance is greater across the boundary than
414 along the boundary, which means that D_{gb} for transport perpendicular to the boundary
415 may be much smaller than D_{gb} parallel to the boundary (Farver and Yund 2000a; Ricoult
416 and Kohlstedt 1983). Diffusion rates measured in grain coarsening experiments are
417 controlled by diffusion in a moving boundary (diffusion across the boundary), whereas
418 the rates obtained from tracer diffusion experiments are related to diffusion along the
419 grain boundary (Ricoult and Kohlstedt 1983). In other words, the diffusion rates inferred
420 from coarsening experiments (Joesten 1983, 1991; Tullis and Yund 1982; this study) are
421 lower than those in tracer diffusion experiments (Farver and Yund 2000a).

422 In the Ag/Au system, the ratio of diffusion rate along the grain boundary to that across
423 the grain boundary varies according to the misorientation angles between neighboring
424 grains, and is less than ~20 (Ma and Balluffi 1993). Based on an analysis of spinel
425 formation between single crystals of periclase and sapphire, Keller et al. (2010) reported
426 that ionic mobility in a polycrystal depends on grain-boundary structures, such as

misorientations between neighboring grains, and that diffusion rates should be low at low-angle grain boundaries with misorientation angles of <15°. They suggested that grain boundary diffusion in spinel varies by one order of magnitude as the misorientation changes from 0° to 60°. For metals and silicates, since the ratio of diffusion rate along the grain boundary to that across the grain boundary varies by one order of magnitude, it seems that anisotropic diffusion at grain boundaries is an important factor in explaining the large difference between the measured silicon grain-boundary diffusion rate and that obtained from grain coarsening studies, although other factors also contribute to the difference.

Grain-size-sensitive creep (diffusion creep or grain-boundary sliding) is governed by diffusion along grain boundaries, which depends on $D_{gb}\delta$ (e.g., Poirier 1985), and is rate limited by the diffusion of Si along the grain boundary, if the slowest-diffusing species is rate controlling (Raj 1982). During deformation, grain-size-sensitive creep and grain growth occur simultaneously (e.g., Platt and Behr 2011), suggesting that diffusion across grain boundaries operates effectively. If the difference between grain-boundary diffusion rates estimated by grain coarsening experiments and by diffusion experiments is caused mainly by the difference in diffusion rates across and along grain boundaries, then grain growth and deformation would be governed by the different temperature-dependent

445 coefficients for grain-boundary diffusion in quartz aggregates. In this case, the 'effective'
446 grain-boundary diffusion rate may be intermediate between the rates of diffusion along
447 and across the grain boundary, and would be higher than the grain-boundary diffusion rate
448 estimated by grain coarsening experiments, and lower than that estimated by tracer
449 diffusion experiments.
450

451 **ACKNOWLEDGMENTS**

452 We thank T. Hirajima for analyzing the carbonaceous material by Raman
453 microspectroscopy at Kyoto University. We are grateful to A. Okamoto for making
454 valuable comments on this study. R. Milke is thanked for his valuable comments on an
455 early version of the manuscript. This paper benefited from detailed reviews by two
456 anonymous referees. Edward Ghent is thanked for his editorial handling of the
457 manuscript.
458

459 **REFERENCES CITED**

460 Aoya, M., Kouketsu, Y., Endo, S., Shimizu, H., Mizukami, T., Nakamura, D., and Wallis,
461 S. (2010) Extending the applicability of the Raman carbonaceous-material
462 geothermometer using data from contact metamorphic rocks. Journal of Metamorphic

463 Geology, 28, 895–914.

464 Béjina, F. and Jaoul, O. (1996) Silicon self-diffusion in quartz and diopside measured by
465 nuclear micro-analysis methods. Physics of the Earth and Planetary Interiors, 97,
466 145–162.

467 Beyssac, O., Goffé, B., Chopin, C., and Rouzaud, J.N. (2002) Raman spectra of
468 carbonaceous material in metasediments: a new geothermometer. Journal of
469 Metamorphic Geology, 20, 859–871.

470 Brodhag, S.H., Herwegh, M., and Berger, A. (2011) Grain coarsening in polymineralic
471 contact metamorphic carbonate rocks: The role of different physical interactions
472 during coarsening. Journal of Structural Geology, 33, 698–712.

473 Dohmen, R. and Milke, R. (2010) Diffusion in polycrystalline materials: Grain
474 boundaries, mathematical models, and experimental data. Reviews in Mineralogy and
475 Geochemistry, 72, 921–970.

476 Farver, J.R. and Yund, R.A. (1991a) Measurement of oxygen grain boundary diffusion in
477 natural, fine-grained, quartz aggregates. Geochimica et Cosmochimica Acta, 55,
478 1597–1607.

479 Farver, J.R. and Yund, R.A. (1991b) Measurement of oxygen diffusion in quartz:
480 Dependence on temperature and water fugacity. Chemical Geology, 90, 55–70.

481 Farver, J. and Yund, R. (2000a) Silicon diffusion in a natural quartz aggregate: constraints
482 on solution-transfer diffusion creep. Tectonophysics, 325, 193–205.
483 Farver, J.R. and Yund, R.A. (2000b) Silicon diffusion in forsterite aggregates:
484 Implications for diffusion accommodated creep. Geophysical Research Letters, 27,
485 2337–2340.
486 Giletti, B.J. and Yund, R.A. (1984) Oxygen diffusion in quartz. Journal of Geophysical
487 Research, 89, 4039–4046.
488 Hanson, R.B. and Barton, M.D. (1989) Thermal development of low-pressure
489 metamorphic belts: Results from two-dimensional numerical models. Journal of
490 Geophysical Research, 94B, 10363–10377.
491 Holland, T.J.B. and Powell, R. (1998) An internally consistent thermodynamic data set
492 for phases of petrological interest. Journal of Metamorphic Geology, 16, 309–343.
493 Herwegh, M., Linckens, J., Ebert, A., Berger, A., and Brodhag, S.H. (2011) The role of
494 second phases for controlling microstructural evolution in polymineralic rocks: A
495 review. Journal of Structural Geology, 33, 1728–1750.
496 Joesten, R. (1983) Grain growth and grain boundary diffusion in quartz from the
497 Christmas Mountains (Texas) contact aureole. American Journal of Science, 283A,
498 233–254.

499 Joesten, R. (1991) Kinetics of coarsening and diffusion-controlled mineral growth.
500 Reviews in Mineralogy, 26, 507–582.
501 Keller, L.M., Götze, L.C., Rybacki, E., Dresen, G., and Abart, R. (2010) Enhancement of
502 solid-state reaction rates by non-hydrostatic stress effects on polycrystalline diffusion
503 kinetics. American Mineralogist, 95, 1399–1407.
504 Kiji, M., Ozawa, H., and Murata, M. (2000) Cretaceous adakitic Tamba granitoids in
505 northern Kyoto, San'yo belt, Southwest Japan. Journal of Mineralogical and
506 Petrological Sciences, 29, 136–149.
507 Kimura, K., Yoshioka, T., Imoto, N., Tanaka, S., Musashino, M., and Takahashi, Y.
508 (1998) Geology of the Kyoto–Tohokubu district (with geological sheet map at
509 1:50,000). Geological Survey of Japan, Tsukuba.
510 Kimura, K., Yoshioka, T., Nakano, S., and Matsuoka, A. (2001) Geology of the
511 Kitakomatsu district (with geological sheet map at 1:50,000). Geological Survey of
512 Japan, Tsukuba.
513 Ma, Q. and Balluffi, R.W. (1993) Diffusion along [001] tilt boundaries in the Au/Ag
514 system 1. Experimental results. Acta Metallurgica et Materialia, 41, 133–141.
515 Milke, R. and Heinrich, W. (2002) Diffusion-controlled growth of wollastonite rims
516 between quartz and calcite: comparison between nature and experiment. Journal of

517 Metamorphic Geology, 20, 467–480.

518 Milke, R. and Wirth, R. (2003) The formation of columnar fiber texture in wollastonite
519 rims by induced stress and implications for diffusion-controlled corona growth.
520 Physics and Chemistry of Minerals, 30, 230–242.

521 Nakashima, S. (1995) Diffusivity of ions in pore water as a quantitative basis for rock
522 deformation rate estimates. Tectonophysics, 245, 185–203.

523 Okudaira, T. and Shigematsu, N. (2012) Estimates of stress and strain rate in mylonites
524 based on the boundary between the fields of grain-size sensitive and insensitive creep.
525 Journal of Geophysical Research, 117, B03210, doi:10.1029/2011JB008799.

526 Okudaira, T., Ogawa, D., and Michibayashi, K. (2010) Grain-size-sensitive deformation
527 of upper greenschist- to lower amphibolite-facies metacherts from a low-*P*/high-*T*
528 metamorphic belt. Tectonophysics, 492, 141–149.

529 Parks, G.A. (1984) Surface and interfacial free energies of quartz. Journal of Geophysical
530 Research, 89B, 3997–4008.

531 Piwinskii, A.J. (1973) Experimental studies of granitoids from the central and southern
532 Coast Ranges, California. Mineralogy and Petrology (Tschermaks Mineralogische
533 und Petrographische Mitteilungen), 20, 107–130.

534 Poirier, J.P. (1985) Creep of Crystals. Cambridge University Press, London.

535 Ricoult, D.L. and Kohlstedt, D.L. (1983) Structural width of low-angle grain boundaries
536 in olivine. Physics and Chemistry of Minerals, 9, 133–138.
537 Raj, R. (1982) Creep in polycrystalline aggregates by matter transport through a liquid
538 phase. Journal of Geophysical Research, 87, 4731–4739.
539 Rubie, D.C. (1986) The catalysis of mineral reactions by water and restrictions on the
540 presence of aqueous fluid during metamorphism. Mineralogical Magazine, 50,
541 399–415.
542 Saal, B., Sockel, H.G., and Heilmaier, M. (1990) Numerical evaluation method for the
543 determination of grain-boundary diffusion coefficients from tracer concentration
544 profiles for a constant boundary concentration. Philosophical Magazine, 61, 801–811.
545 Shen, A.H., Bassett, W.A., and Chou, I.-M. (1993) The α-β transition at high
546 temperatures and pressures in a diamond-anvil cell by laser interferometry. American
547 Mineralogist, 78, 694–698.
548 Shimojuku, A., Kubo, T., Ohtani, E., Nakamura, T., Okazaki, R., Dohmen, R., and
549 Chakraborty, S. (2009) Si and O diffusion in $(Mg,Fe)_2SiO_4$ wadsleyite and
550 ringwoodite and its implications for the rheology of the mantle transition zone. Earth
551 and Planetary Science Letters, 284, 103–112.
552 Tullis, J. and Yund, R.A. (1982) Grain growth kinetics of quartz and calcite aggregates.

553 Journal of Geology, 90, 301–318.

554 Turcotte, D.L. and Schubert, G. (1982) Geodynamics. John Wiley and Sons, New York.

555 Watson, E.B. (1991) Diffusion in fluid-bearing and slightly-melted rocks: experimental
556 and numerical approaches illustrated by iron transport in dunite. Contributions to
557 Mineralogy and Petrology, 107, 417–434.

558 Wells, P.R.A. (1980) Thermal models for the magmatic accretion and subsequent
559 metamorphism of continental crust. Earth and Planetary Science Letters, 46, 253–265.

560 Yamazaki, D., Kato, T., Yurimoto, H., Ohtani, E., and Toriumi, M. (2000) Silicon
561 self-diffusion in $MgSiO_3$ perovskite at 25 GPa. Physics of the Earth and Planetary
562 Interiors, 119, 299–309.

563

564 **FIGURE CAPTIONS**

565 **FIGURE 1.** Geological map for the Hanase–Bessho quartz diorite and surrounding
566 areas. The map was compiled during this study with the help of data from Kimura et al.
567 (1998, 2001). Localities of metachert samples (solid circles) and metapelite samples
568 (open circles) are shown. Numbers with a dash denote samples 120322-#, and those
569 without a dash, samples 110331-#.

570 **FIGURE 2.** Temperature profiles showing the thermal evolution in and around the
571 Hanase–Bessho quartz diorite after its intrusion. (**a**) Temperature profiles from 0 to 24
572 kyr (2 kyr intervals). (**b**) Maximum temperatures experienced after the intrusion. The
573 temperatures are estimated from the degree of graphitization of carbonaceous material in
574 metapelites, using Raman microspectroscopy.

575 **FIGURE 3.** Microstructures of the metacherts. (**a**) Photomicrographs of samples
576 120322-02 (crossed-polarized light) and 110331-15 (back-scattered electron image,
577 shadow mode). (**b**) Grain size distribution of quartz grain sizes for samples 120322-02
578 and 110331-15.

579 **FIGURE 4.** Grain size variation plotted against the distance from the intrusive contact.

580 **FIGURE 5.** Arrhenius plot of $\ln[(d^2 - d_0^2)T]$ versus $1/T$. The solid lines (1) and (2) are
581 linear least squares fits for 17 data points (solid circles + open circles) and for 14 data

582 points (solid circles), respectively. See the text for details.

583 **FIGURE 6.** Calculated and measured grain size variations. $D_{Si,\ bulk}$ (wet, FY00), $D_{Si,\ bulk}$
584 (dry, FY00), D_{gb} (J83), and "this study" represent, respectively, the grain size variations
585 using the values of activation energy and pre-exponential factor from Farver and Yund
586 (2000a) for hydrothermal and dry experiments, Joesten (1983), and as estimated by us in
587 this study. The curves (1) and (2) show calculated grain size variations using the values of
588 17 metachert samples and of 14 samples that excluded three samples near the intrusion
589 contact (open circles), respectively.

590 **FIGURE 7.** Comparison of grain-boundary or bulk diffusion rates for quartz aggregates
591 obtained in the present study and in previous studies. $D_{Si,gb\ or\ bulk}$ (wet, FY00), $D_{Si,gb\ or\ bulk}$
592 (dry, FY00), D_{gb} (TY82), D_{gb} (J83), and "this study" denote, respectively, the diffusion
593 rates calculated using the values of activation energy and pre-exponential factor from
594 Farver and Yund (2000a) for hydrothermal and dry experiments, Tullis and Yund (1982),
595 with their values recalculated by Joesten (1991), Joesten (1983), and as estimated by us in
596 this paper. Silicon grain-boundary diffusion rates ($D_{Si,gb}$) were estimated using the
597 relation $D_{Si,bulk} = \tau D_{Si,gb}\delta/d$, where $D_{Si,bulk}$ is the silicon bulk diffusion rate, τ is the
598 tortuosity factor (1.7), δ the grain-boundary width (1 nm), and d the average grain size (10
599 μm). Diffusion rates represented by thick lines are those calculated for the experimental

600 temperature range, and those represented by thin lines are the extrapolated rates for the
601 entire temperature range. The labels “this study, 17” and “this study, 14” represent
602 diffusion rates calculated using the activation energy and the pre-exponential factor
603 estimated based on 17 metachert samples and on 14 samples (excluding three samples
604 from near the intrusion contact), respectively. Also shown are the volume diffusion rates
605 of O in α- and β-quartz under hydrothermal conditions (Farver and Yund 1991b; Giletti
606 and Yund 1984), and of Si in β-quartz (Béjina and Jaoul 1996).

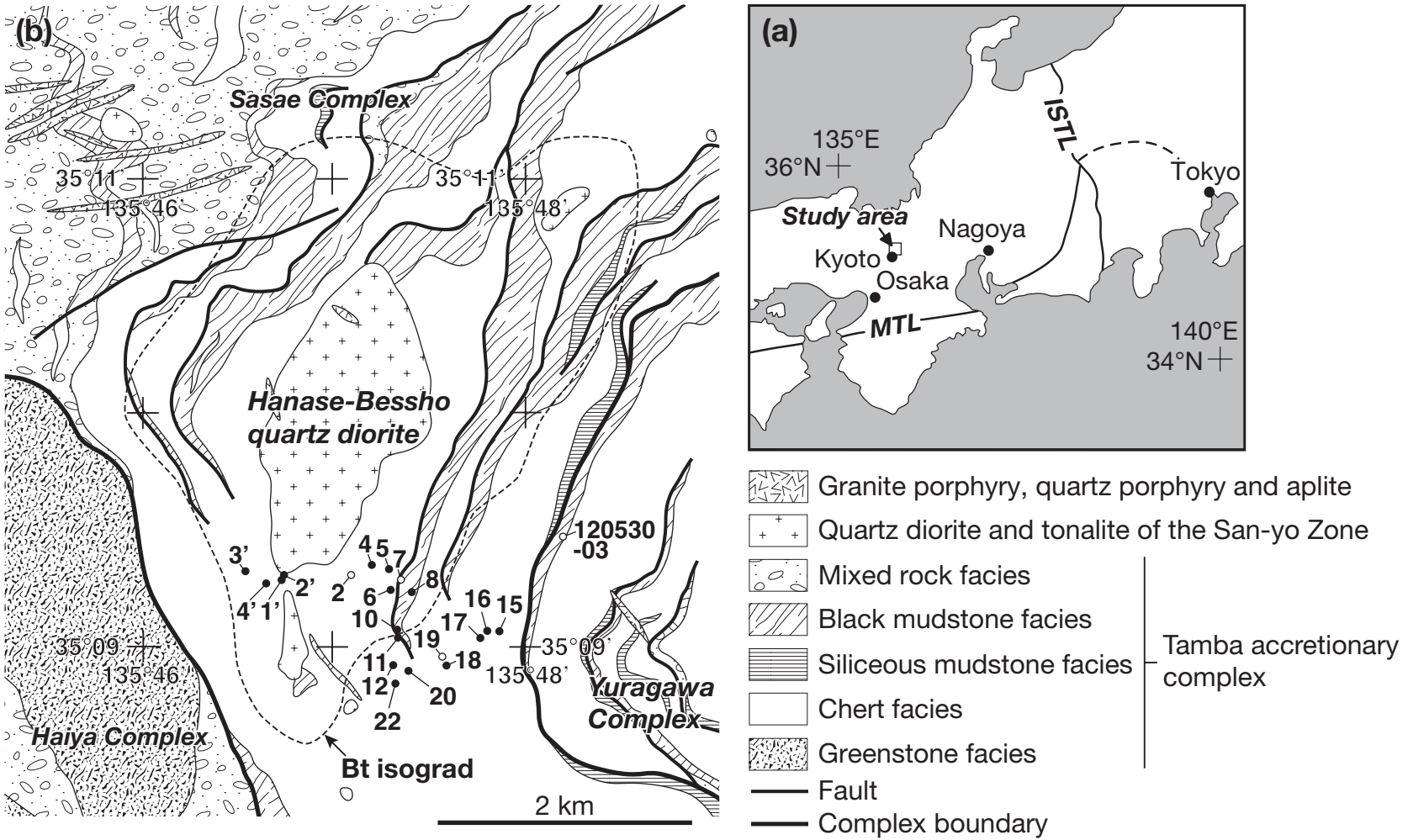
(b)
Sasae Complex
35°11′
135°46′
35°11′
135°48′
Hanase-Bessho
quartz diorite
120530
-03
3′
4
5
7
8
2′
2
6
4′
1′
10
16
15
17
19
18
11
12
20
22
35°09′
135°46′
35°09′
135°48′
Yuragawa
Complex
Haiya Complex
Bt isograd
2 km
(a)
ISTL
135°E
36°N
Tokyo
Study area
Nagoya
Kyoto
Osaka
MTL
140°E
34°N
Granite porphyry, quartz porphyry and aplite
Quartz diorite and tonalite of the San-yo Zone
Mixed rock facies
Black mudstone facies
Siliceous mudstone facies
Chert facies
Greenstone facies
Tamba accretionary complex
Fault
Complex boundary

Figure 1

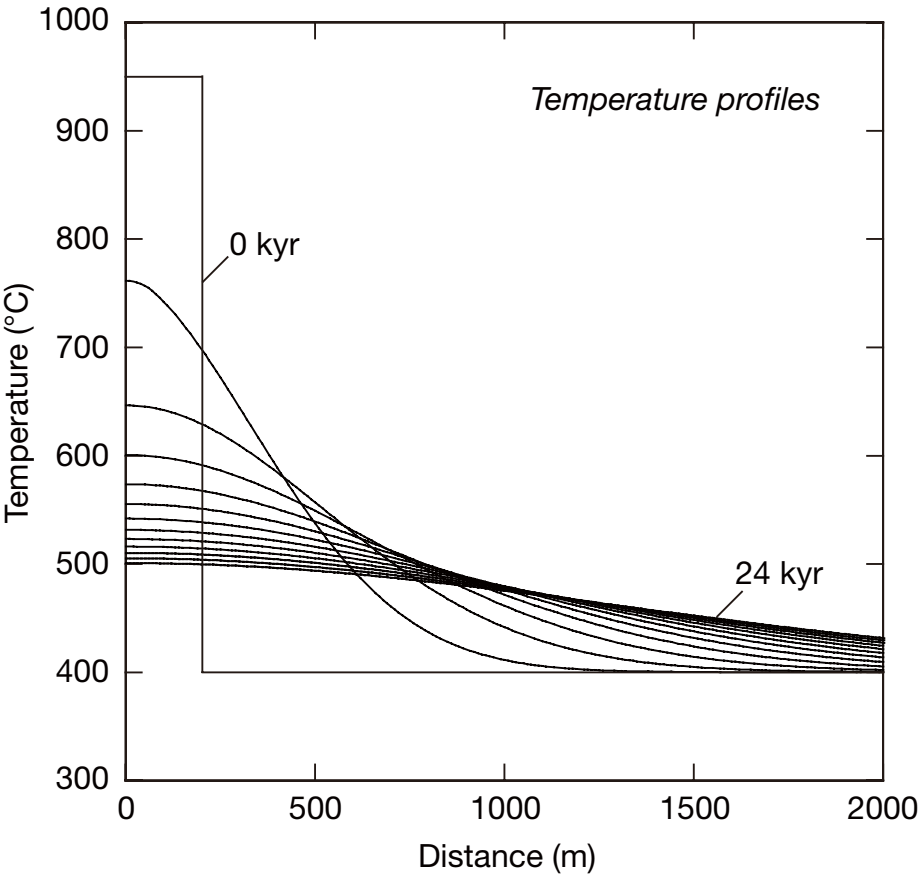
Temperature profiles
0 kyr
24 kyr
Temperature (°C)
Distance (m)
1000
900
800
700
600
500
400
300
0
500
1000
1500
2000

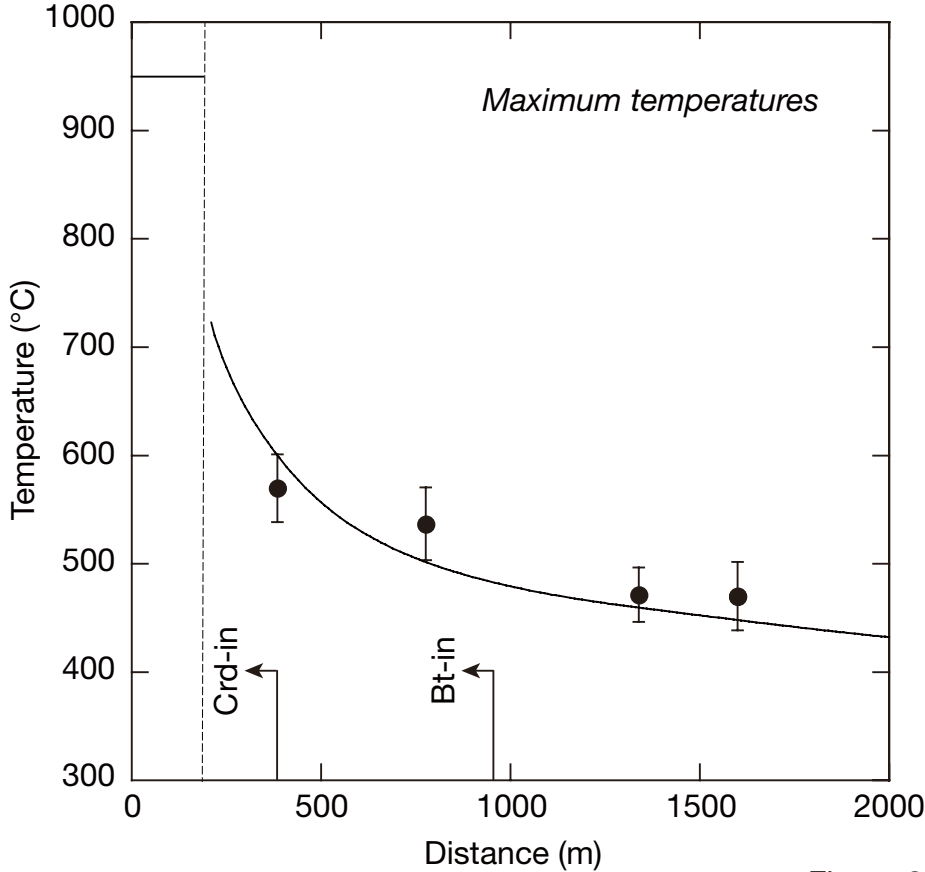
Maximum temperatures
Crd-in
Bt-in
Temperature (°C)
Distance (m)
1000
900
800
700
600
500
400
300
0
500
1000
1500
2000

Figure 2

(a) Microstructure

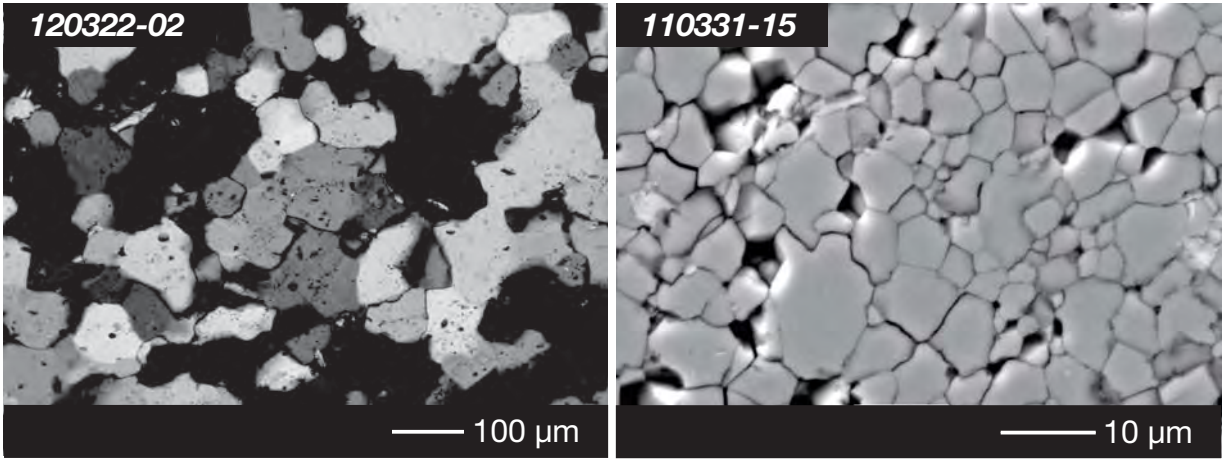

(b) Grain size distribution

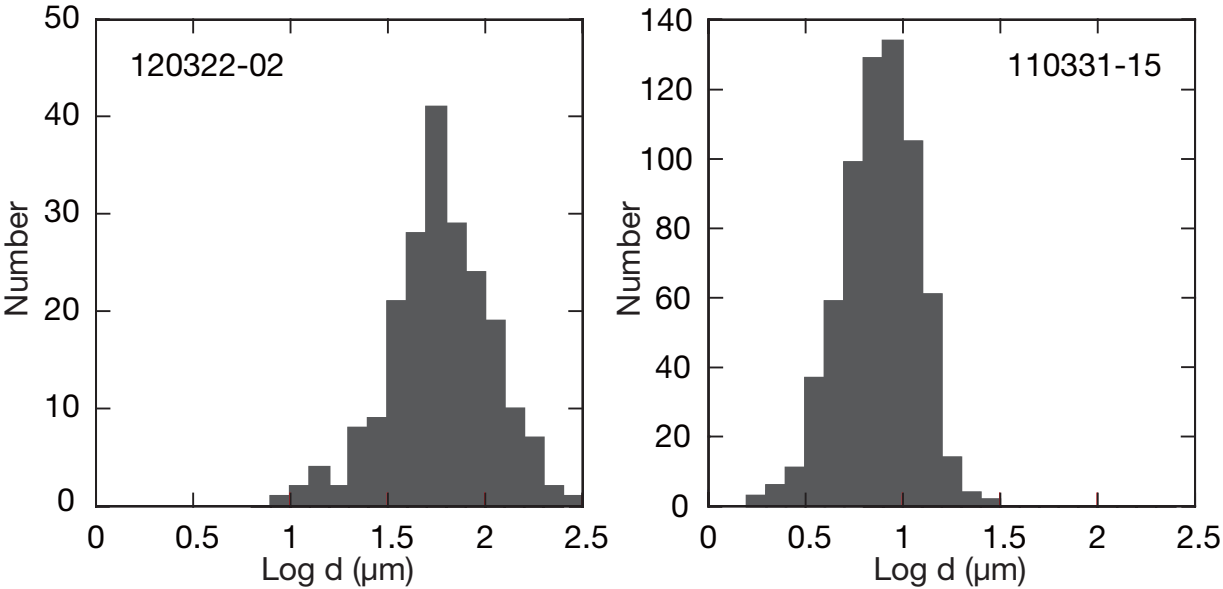

Figure 3

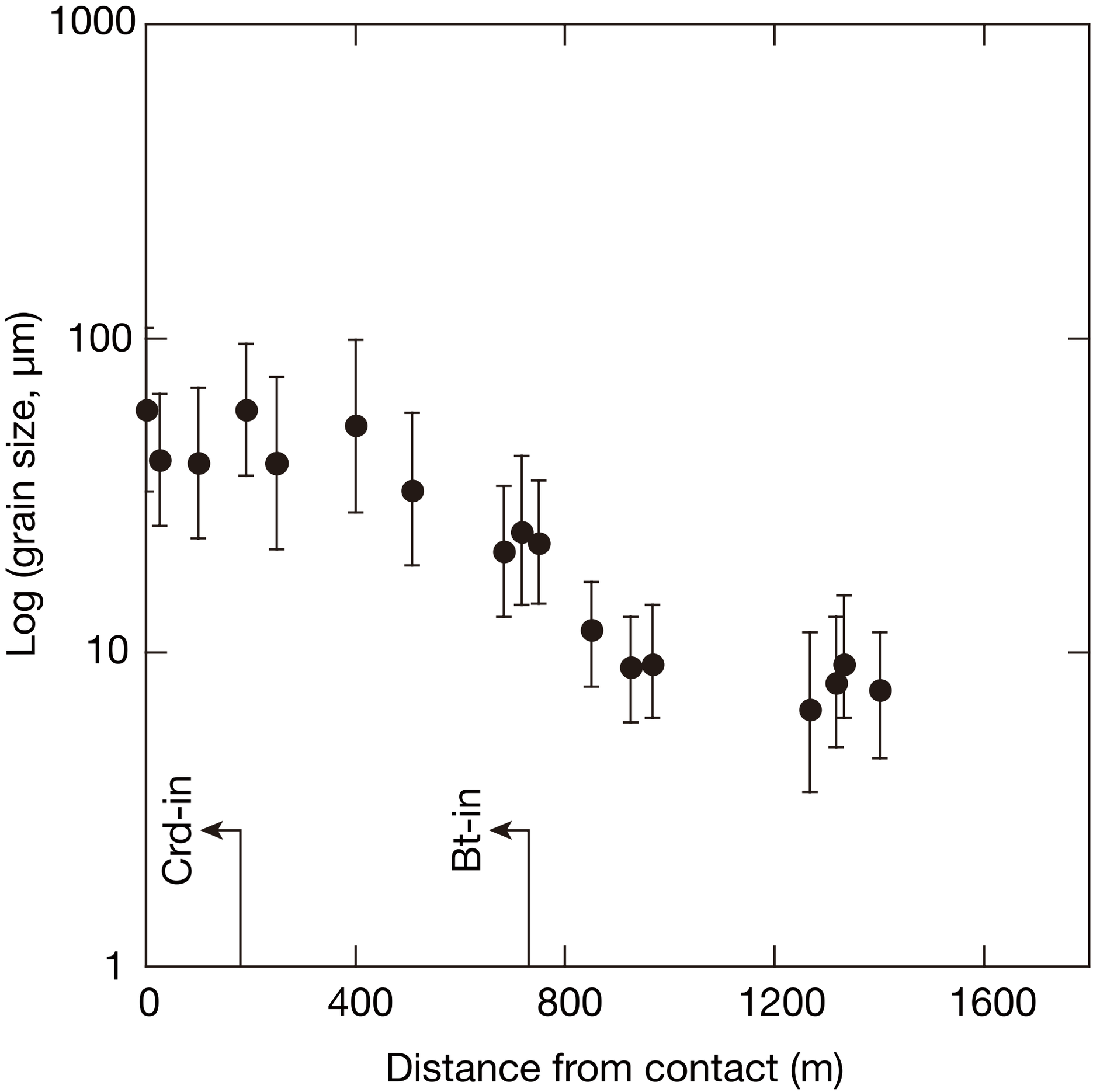
1000
100
10
1
Log (grain size, μm)
0
400
800
1200
1600
Distance from contact (m)
Crd-in
Bt-in

Figure 4

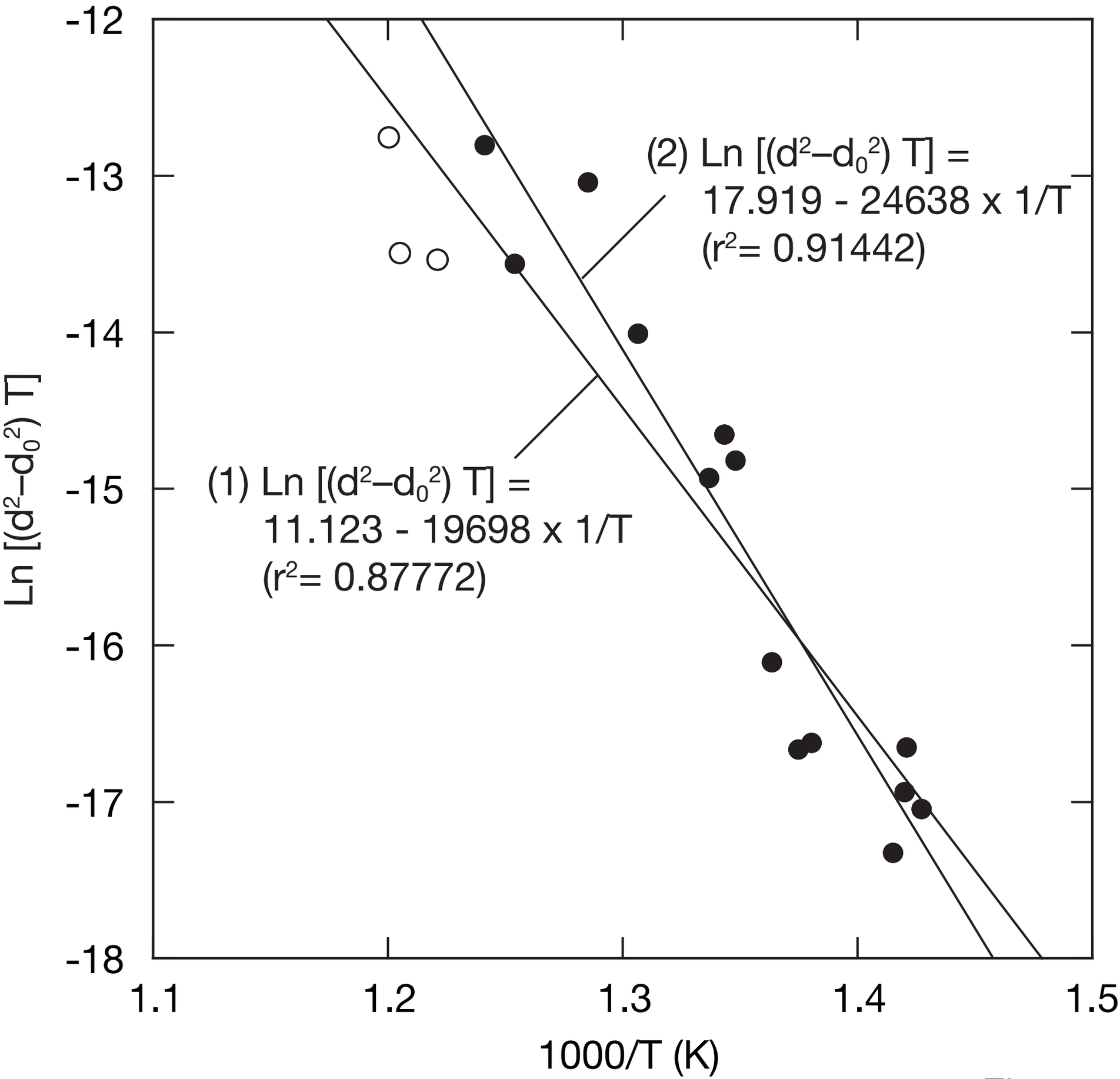
-12
-13
-14
-15
-16
-17
-18
Ln [(d²–d₀²) T]
1.1
1.2
1.3
1.4
1.5
1000/T (K)
(2) Ln [(d²–d₀²) T] =
17.919 - 24638 x 1/T
(r²= 0.91442)
(1) Ln [(d²–d₀²) T] =
11.123 - 19698 x 1/T
(r²= 0.87772)

Figure 5

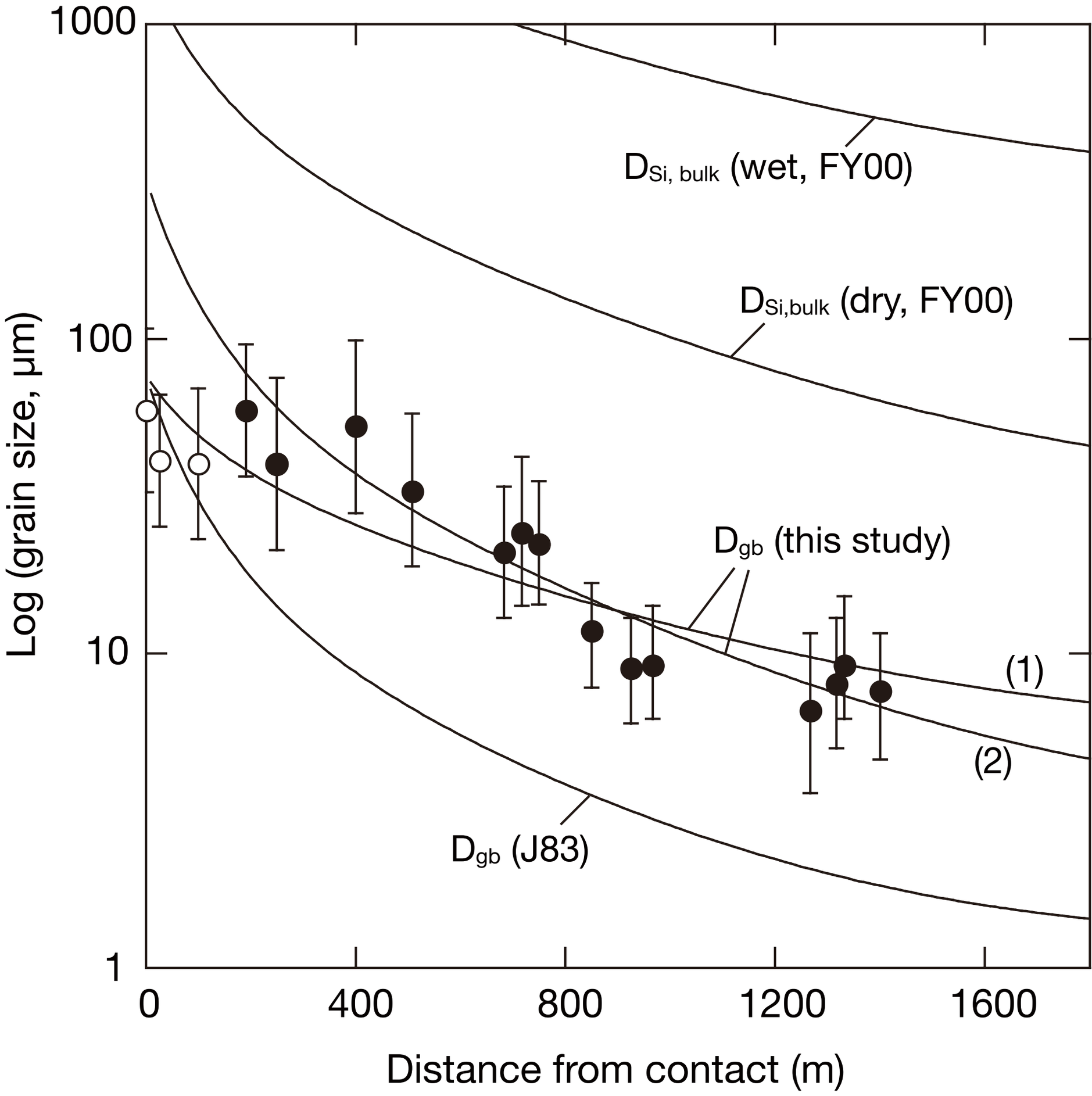
1000
100
10
1
Log (grain size, μm)
0
400
800
1200
1600
Distance from contact (m)
$D_{Si,\ bulk}$ (wet, FY00)
$D_{Si,bulk}$ (dry, FY00)
D_{gb} (this study)
(1)
(2)
D_{gb} (J83)

Figure 6

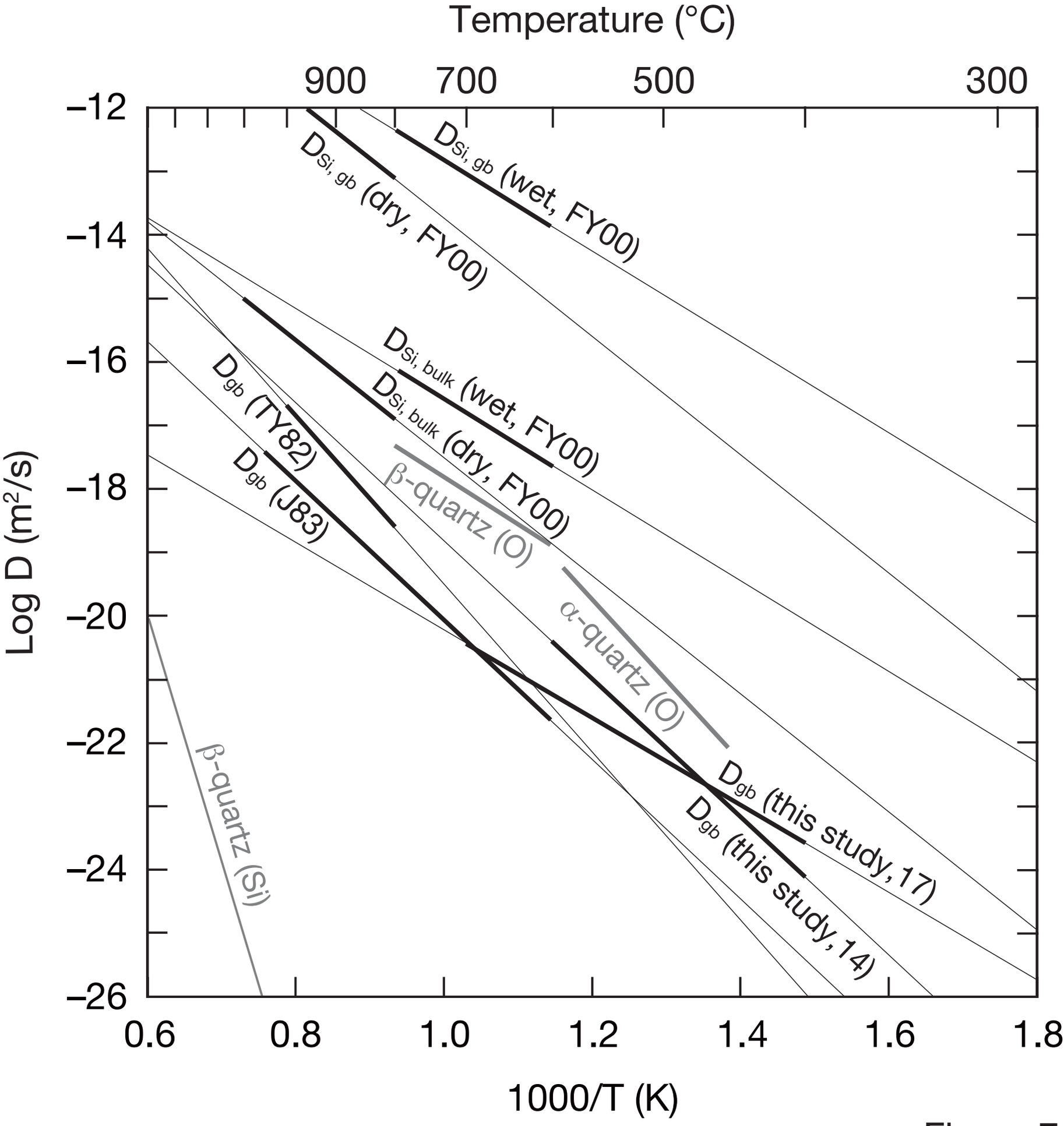
Temperature (°C)
900
700
500
300
−12
−14
−16
−18
−20
−22
−24
−26
Log D (m²/s)
0.6
0.8
1.0
1.2
1.4
1.6
1.8
1000/T (K)
Dsi, gb (wet, FY00)
Dsi, gb (dry, FY00)
Dsi, bulk (wet, FY00)
Dsi, bulk (dry, FY00)
Dgb (TY82)
Dgb (J83)
β-quartz (O)
α-quartz (O)
β-quartz (Si)
Dgb (this study, 17)
Dgb (this study, 14)

Figure 7

TABLE 1. Parameters used in numerical simulations for the thermal modeling and grain growth modeling

Parameters used in the thermal modeling	
Density of rock (ρ_m)	2750 kg/m^3 [1]
Specific heat of rock (C_m)	880 J/kg/K [1]
Thermal conductivity (K)	2.8 W/m/K [1]
Heat produced by radioactive elements (A)	2.64×10^{-6} W/m^3 [1]
Initial temperature of the intrusion (T_{int})	950 °C
Solidus temperature of the intrusion (T_{sol})	750 °C [2]
Liquidus temperature of the intrusion (T_{liq})	1050 °C [2]
Initial temperature of the country rocks	350 °C
Enthalpy of crystallizing magma (ΔH_{magma})	3.35×10^5 J/kg [3, 4]
Parameters used in the grain growth modeling	
Surface free energy (γ) of quartz	0.4 J/m^2 [5]
Molar volume (V) of quartz	2.269×10^{-5} m^3/mol [6]
Grain-boundary width (δ)	1×10^{-9} m

References: [1] Turcotte and Schubert (1982); [2] Piwinskii (1973); [3] Wells (1980); [4] Hanson and Barton (1989); [5] Parks (1984); [6] Holland and Powell (1998)

TABLE 2. Results of quartz grain size analysis

Sample	Distance* (m)	N	Grain size (μm)	–1 σ/+1 σ	2nd-phases (vol.%)
120322-02	1	208	59.0	26.6/4836	3.0
120322-01	27	356	40.9	15.4/24.9	4.2
120322-04	100	356	40.3	16.0/26.6	2.3
120322-03	191	298	58.6	22.6/36.7	0.9
110331-04	250	617	40.3	18.7/34.7	0.5
110331-05	400	856	52.9	24.7/46.4	0.1
110331-06	508	509	32.9	14.1/24.7	1.9
110331-08	683	625	21.0	8.0/13.1	1.4
110331-10	717	533	24.2	10.3/17.8	0.3
110331-11	750	499	22.3	8.4/13.4	0.7
110331-12	850	671	11.8	3.7/5.5	0.8
110331-22	925	614	9.0	3.0/4.4	7.2
110331-20	967	881	9.2	3.2/4.9	1.7
110331-18	1267	700	6.6	3.0/5.5	1.6
110331-17	1317	475	8.0	3.1/5.0	0.2
110331-16	1333	564	9.2	3.5/5.6	0.8
110331-15	1400	665	7.6	2.7/4.3	0.1

* Distance is measured from the intrusion contact.

TABLE 3 Mean R2 values and estimated temperatures by Raman spectral analysis

Sample	Distance* (m)	N	R2 ratio (±1 σ)	$T^{[1]}$ (°C)	$T^{[2]}$ (°C)
110331-02	182	28	0.138±0.073	570±32	578±41
110331-07	573	28	0.222±0.076	536±34	537±38
110331-19	1136	13	0.375±0.057	471±25	463±27
120530-03	1400	26	0.376±0.071	470±32	461±33

* Distance is measured from the intrusion contact.

References: [1] Beyssac et al. (2002); [2] Aoya et al. (2010)